OPEN ACCESS
CellPress

Cell Reports
Resource

Multilayered Control of Protein Turnover by TORC1 and Atg1

Zehan Hu,[1,3] Serena Raucci,[1,3] Malika Jaquenoud,[1] Riko Hatakeyama,[1] Michael Stumpe,[1] Rudolf Rohr,[1] Fulvio Reggiori,[2] Claudio De Virgilio,[1,*] and Jörn Dengjel[1,4,*]
[1]Department of Biology, University of Fribourg, 1700 Fribourg, Switzerland
[2]Department of Biomedical Sciences of Cells & Systems, University of Groningen, University Medical Center Groningen, 9713 AV Groningen, the Netherlands
[3]These authors contributed equally
[4]Lead Contact
*Correspondence: claudio.devirgilio@unifr.ch (C.D.V.), joern.dengjel@unifr.ch (J.D.)
https://doi.org/10.1016/j.celrep.2019.08.069

SUMMARY

The target of rapamycin complex 1 (TORC1) is a master regulator of cell homeostasis, which promotes anabolic reactions and synchronously inhibits catabolic processes such as autophagy-mediated protein degradation. Its prime autophagy target is Atg13, a subunit of the Atg1 kinase complex that acts as the gatekeeper of canonical autophagy. To study whether the activities of TORC1 and Atg1 are coupled through additional, more intricate control mechanisms than simply this linear pathway, we analyzed the epistatic relationship between TORC1 and Atg1 by using quantitative phosphoproteomics. Our *in vivo* data, combined with targeted *in vitro* TORC1 and Atg1 kinase assays, not only uncover numerous TORC1 and Atg1 effectors, but also suggest distinct bi-directional regulatory feedback loops and characterize Atg29 as a commonly regulated downstream target of both TORC1 and Atg1. Thus, an exquisitely multilayered regulatory network appears to coordinate TORC1 and Atg1 activities to robustly tune autophagy in response to nutritional cues.

INTRODUCTION

Cells continually adapt their metabolisms to meet nutrient and energy requirements in response to environmental cues. The target of rapamycin complex 1 (TORC1) signaling pathway plays a key role in homeostatically regulating metabolism, cell growth, and proliferation in response to nutrients and growth factors (Albert and Hall, 2015; Saxton and Sabatini, 2017). Under conditions that promote growth, the TORC1 protein kinase stimulates protein synthesis and inhibits protein degradation via macroautophagy (hereafter referred to as autophagy) (Dikic and Elazar, 2018; Hurley and Young, 2017; Kamada et al., 2010). Nutrient limitation, in turn, results in TORC1 inhibition and, consequently, the induction of autophagy, an evolutionarily conserved catabolic process. Autophagy critically contributes to cell survival through the recycling of macromolecular complexes and the removal of nonfunctional and potentially toxic cellular components by autophagosome-mediated vacuolar or lysosomal degradation (Mizushima et al., 2011).

In yeast, more than 42 autophagy-related (Atg) proteins are critical for vacuolar targeting of cytoplasmic components (Dikic and Elazar, 2018). Several of them are part of five conserved protein complexes that form the core Atg machinery (Klionsky et al., 2011): (1) the Atg1 kinase complex (comprising Atg1, Atg13, Atg17, Atg29, and Atg31), which is critical for autophagy initiation; (2) the class III phosphatidylinositol 3-kinase complex (comprising Vps34, Vps15, Atg6, and Atg14), which generates the lipid phosphatidylinositol-3-phosphate that serves as the docking site for protein recruitment; (3) the Atg9 cycling system (comprising Atg9, Atg2, and Atg18), which provides part of the vesicles for autophagosome generation; (4) the Atg12 ubiquitin-like conjugation system (comprising Atg7, Atg10, Atg5, and Atg16), which generates the Atg12-Atg5/Atg16 complex that has E3 enzyme-like activity toward Atg8; and (5) the Atg8 ubiquitin-like conjugation system (comprising Atg7, Atg3, and Atg8), which leads to the conjugation of Atg8 to phosphatidylethanolamine, with Atg8 being critical for phagophore expansion and cargo recruitment (Dikic and Elazar, 2018).

TORC1 controls autophagy by directly impinging on the yeast Atg1 and mammalian ULK1 kinase complexes. In yeast, TORC1 inhibits Atg1 kinase activity and, consequently, autophagy by directly phosphorylating the Atg1 kinase complex subunit Atg13 (Kamada et al., 2000, 2010). In mammals, mTORC1 phosphorylates both ATG13 and ULK1 (Hosokawa et al., 2009; Jung et al., 2009; Kim et al., 2011). Current knowledge suggests a simple linear relationship between TORC1 and Atg1. However, regulatory modules that critically define cellular fitness are often embedded into multilayered mechanisms that ensure robust cellular responses. Accordingly, robustness can be generated by redundancies and inbuilt cross-communication between elements of signaling pathways, which ensure that only stimuli of the appropriate strength and duration are able to turn on or off their respective cellular responses (Azeloglu and Iyengar, 2015). Whether TORC1 and Atg1 are more intricately interconnected through such mechanisms is largely unanswered. In part, this is because the compendium of TORC1 and Atg1 target residues is currently incomplete. To address this outstanding issue, we decided to develop a mass spectrometry (MS)-based phosphoproteomics strategy that combines global proteomics

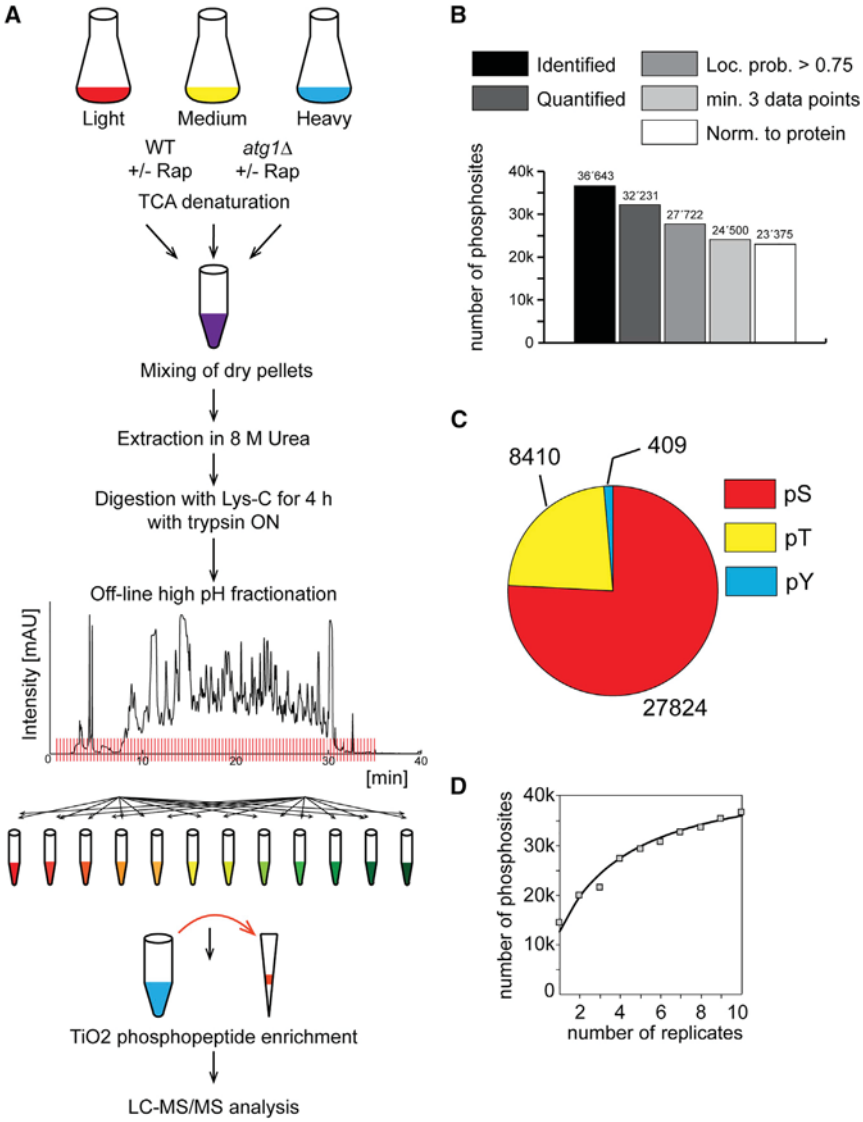

Figure 1. Quantitative Phosphoproteomics Analyses of Rapamycin-Treated Yeast Cells

(A) Quantitative MS-based proteomics workflow. Yeast cells were labeled by Lys0, Arg0 (light), Lys4, Arg6 (medium), or Lys8 Arg10 (heavy) amino acid variants.

(B) Identified and quantified phosphosites of all 10 SILAC experiments. Data-filtering steps are indicated.

(C) Pie chart of identified pSer, pThr, and pTyr sites.

(D) Cumulatively identified phosphosites in 10 SILAC experiments indicate the saturation of identifiable phosphorylation sites. Identified site numbers (gray squares) were fitted with the least square optimization predicting a maximum number of identifications of 45,109 sites (black line). See also Figure S1.

screens *in vivo* with targeted *in vitro* protein kinase assays. Specifically, we present here the currently largest set of TORC1-dependent phosphorylation events in the yeast *Saccharomyces cerevisiae*; identify numerous hitherto unknown TORC1 and Atg1 effectors; and characterize functionally relevant, new TORC1 target sites on Atg1 complex subunits. Our combined data highlight the existence of a sophisticated network of bi-directional regulatory feedback loops and nodes of convergence between TORC1 and Atg1, indicating that these signaling hubs are much more intricately interconnected than previously realized.

RESULTS

The Rapamycin-Sensitive Phosphoproteome: Modulation of Pathways Controlling Protein Homeostasis

To cover comprehensively the potential TORC1 and Atg1 target sites, we performed a set of 10 stable isotope labeling by amino acids in cell culture (SILAC)-based quantitative phosphoproteomics experiments comparing wild-type (WT) and *atg1*Δ cells in the presence and absence of the highly specific allosteric TORC1 inhibitor rapamycin (Bentley and Banker, 2015; Harding et al., 1989; Heitman et al., 1991; Yang et al., 2013). Differentially labeled cells were treated, or untreated, for 30 min with rapamycin before mixing pellets and processing phosphopeptides for MS/MS analysis (Batth et al., 2014) (Figure 1A; see STAR Methods for details). The 10 SILAC experiments recorded five biological replicates, each comparing the responses of WT and *atg1*Δ cells to rapamycin treatment (Figures S1A and S1B). In total, we identified more than 36,600 phosphosites on 3,508 proteins (Figure 1B)—on average, more than 20,000 sites per experiment. Of these modifications, 76% were on serines, 23% on threonines, and 1% on tyrosines, which is congruent with published data (Batth et al., 2018; Paulo and Gygi, 2015) (Figure 1C). The number of newly identified sites per replicate indicated that we approached saturation, and we estimate that our experimental setup would allow us to identify a maximum of about 45,000 phosphorylation sites (Figure 1D; see STAR Methods for details). Thus, our dataset appears to cover more than 80% of the detectable yeast phosphoproteome.

Of the 36,600 identified sites, more than 32,000 were quantified (Figure 1B). To identify robust phosphorylation-based responses to rapamycin treatment, we stringently filtered the generated data: sites had to be localized to a specific amino acid residue with a probability >0.75 (class I sites according to Olsen et al. [2006]); had to be quantified in a minimum of three biological replicates; and were normalized to respective protein abundances to separate regulated phosphosites from regulated proteins. A total of 23,375 phosphosites fulfilled these criteria (Figure 1B; Table S1).

To identify sites that exhibited a significant fold change in phosphorylation due to rapamycin treatment, we generated a statistical model combining all the biological replicates and sites into a single analysis. The SILAC experiments were split into two groups to identify (1) potential TORC1-regulated sites that responded negatively to rapamycin treatment and (2) potential Atg1-regulated sites that responded positively to rapamycin treatment. TORC1 sites had to be significantly downregulated in WT cells plus rapamycin compared to WT cells minus rapamycin (I in Figure 3), *atg1*Δ cells plus rapamycin compared to *atg1*Δ cells minus rapamycin (II in Figure 3), and WT cells plus rapamycin compared to *atg1*Δ cells minus rapamycin (III in Figure 3). Atg1 sites had to be significantly upregulated in (I), (III), and (IV) WT cells plus rapamycin compared to *atg1*Δ cells plus rapamycin. In addition, Atg1 sites should exhibit no change or a significantly smaller change in experiment (2) compared to (1). As five biological replicates per condition were performed, 15 replicates per protein kinase were used to identify significantly regulated sites. Specifically, we used a random effect model considering the variability among biological replicates, among sites, as well as the number of replicates for each site. Next, the average fold changes and their corresponding 95% confidence intervals were extracted for each site (Figure 2A). This led to a final list of 586 sites (on 309 proteins) and 162 sites (on 128 proteins) that were significantly down- and upregulated by rapamycin treatment, respectively (min. average fold change of 2; $p < 0.05$; Table S1). This list included less than 2.5% of the quantified phosphosites, which reflects the stringent criteria used for defining robust phosphorylation-based signaling responses to rapamycin treatment. Notably, our data cover on average 76% (67%–85%; Figure S1C) of all quantified phosphosites in similar phosphoproteomics datasets (Iesmantavicius et al., 2014; Oliveira et al., 2015; Paulo and Gygi, 2015; Soulard et al., 2010) and list 14,599 additional, hitherto unknown phosphorylation events. Our study further corroborates, on average, 12% of the reported rapamycin-sensitive sites (4%–15%; Figure S1D). Importantly, our study overlaps to a larger extent with published datasets than the respective datasets with one another when considering the total number of rapamycin-sensitive sites.

Virtually all of the previously known proximal TORC1 targets were identified as rapamycin-sensitive, including Atg13 (Kamada et al., 2010), Lst4 (Péli-Gulli et al., 2017), Sch9 (Urban et al., 2007), Sfp1 (Lempiäinen et al., 2009), Ypk3 (González et al., 2015; Yerlikaya et al., 2016), and Vps27 (Hatakeyama et al., 2019) (Table S2). In addition, we detected numerous potential TORC1 target residues within the TORC1 subunit Tco89 (Reinke et al., 2004), which reveals that TORC1 undergoes extensive autophosphorylation. Analyzing the amino acid sequences flanking the regulated phosphosites of potential TORC1 targets, we found similarities to the published yeast and human consensus phosphorylation motifs with proline, aliphatic, or aromatic residues in position +1 (Kang et al., 2013; Mok et al., 2010; Oliveira et al., 2015; Urban et al., 2007) (Figure 2B). The two arginine residues in positions −3 and −2 perfectly match with a consensus phosphorylation site assigned to the direct TORC1 target and protein kinase Sch9 (Huber et al., 2009), indicating that our dataset probably contains Sch9 substrates (see below).

Among the proteins that are phosphorylated in an Atg1-dependent manner in rapamycin-treated cells, our analyses gratifyingly distinguished the known Atg1 target proteins Atg2, Atg9, and Atg29 (Mao et al., 2013; Papinski et al., 2014). Moreover, the Atg1 consensus motif analysis infers aliphatic amino acid residues in position −3 (Figure 2B), which matches well with the previously proposed Atg1/ULK1 motifs (Egan et al., 2015; Papinski et al., 2014). Thus, our data appear to be of high quality, as they largely confirm current knowledge.

To get a global overview of TORC1- and Atg1-regulated signaling pathways and cellular processes, we next performed Gene Ontology (GO) term enrichment analyses of proteins carrying regulated phosphosites. Potential TORC1 targets were significantly enriched in proteins involved in metabolic processes and positive regulation of gene expression ($p < 0.05$, Bonferroni corrected; Figure 2C; Table S3). Potential Atg1 targets were significantly enriched in proteins involved in retrograde transport and autophagy (Figure 2C; Table S3). Besides corroborating the known cellular functions, our data indicate that both kinase complexes control additional processes that are important for protein homeostasis (e.g., transcription and vacuole organization). Interestingly, we also identified a significant enrichment of regulated sites on protein kinases, indicating that rapamycin treatment modulates the activities of protein kinases other than solely TORC1 and Atg1, which is also suggested by our motif analysis (see above; Figures 2B and 2C). To pinpoint new TORC1 effector and/or target kinases, we isolated enriched linear phosphorylation motifs from the rapamycin-sensitive phosphorylation sites and used KinomeXplorer to identify kinases capable of phosphorylating them (Figure 2D) (Horn et al., 2014). We identified four and five motifs within the down- and upregulated sites, respectively. Expectedly, rapamycin appeared to have negative effects on Sch9 and the protein kinase A isoforms Tpk1 and Tpk2 (Soulard et al., 2010; Urban et al., 2007). Also, the known TORC1 downstream effector Gcn2 was identified in these analyses (Cherkasova and Hinnebusch, 2003). Interestingly, next to Atg1, the DNA-damage-responsive, phosphatidylinositol-kinase-related kinases Mec1 and Tel1 appeared to be capable of phosphorylating sites upregulated by rapamycin treatment (Figure 2D). Mec1 has recently been shown to be critical for both the induction of autophagy after genotoxic treatment and for glucose starvation-induced autophagy (Eapen et al., 2017; Yi et al., 2017). Our data therefore suggest that Mec1 and Tel1 may be able to act in concert with or take over Atg1 functions under specific conditions (Corcoles-Saez et al., 2018). The extensive effects of rapamycin treatment on the kinome inspired us to perform a more detailed analysis of protein kinases carrying regulated phosphosites that may be functionally relevant.

TORC1 and Atg1 Regulate Cell Homeostasis through a Highly Cross-Connected Network of Protein Kinases

In total, we identified 23 protein and 3 lipid kinases harboring defined phosphoresidues that are significantly regulated by either TORC1 or Atg1 (Figure 3). Of the ones regulated by TORC1, Sch9 and Ypk3 are bona fide proximal targets (González et al., 2015; Martin et al., 2004; Urban et al., 2007; Yerlikaya et al., 2016), while Npr1 and Gcn2 have been described as distally

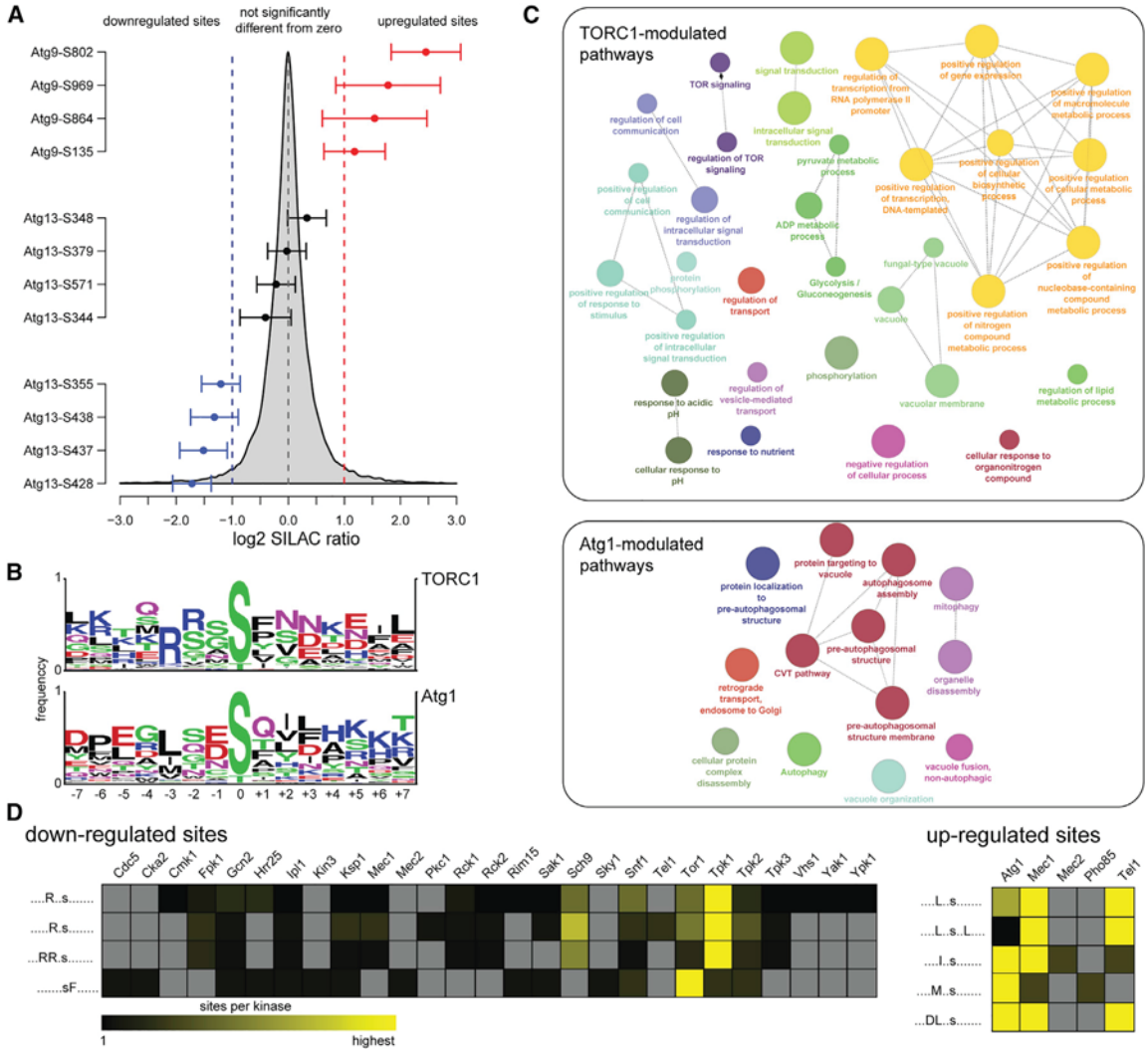

Figure 2. The Rapamycin-Sensitive Phosphoproteome

(A) Statistical approach for the identification of significant regulated phosphosites by rapamycin treatment. The gray curve indicates the SILAC ratio distribution of 23,375 phosphosites, comparing cells grown in the presence and absence of rapamycin (30 min). As an example for regulated and non-regulated sites, 12 sites are shown with their average values and confidence intervals. Blue sites are significantly downregulated, and red sites are significantly upregulated by rapamycin treatment ($p > 0.05$). Two-fold cutoff values are marked by colored dashed lines.

(B) Motif analyses of potential TORC1 and Atg1 phosphosites responding minimally 2-fold to rapamycin treatment. Potential TORC1 sites are downregulated, and potential Atg1 sites are upregulated by rapamycin treatment.

(C) GO term enrichment analysis of proteins carrying positive and negative regulated phosphosites highlights perturbed cell homeostasis.

(D) Motif analyses and predictions of kinases potentially being perturbed by rapamycin treatment.

See also Figure S1.

controlled by TORC1 (Garcia-Barrio et al., 2002; Schmidt et al., 1998). In addition, several of the other TORC1-controlled protein kinases have previously been found to be part of the TORC1-associated protein kinase network (Breitkreutz et al., 2010), including Bck1, Ksp1, and Sky1, which were also linked to autophagic processes (Krause and Gray, 2002; Manjithaya et al., 2010; Rodríguez-Lombardero et al., 2014; Umekawa and Klionsky, 2012). Besides precisely pinpointing the phosphorylation events that are likely functionally relevant for processing signals that emanate from TORC1, these findings uncover the existence of multiple regulatory layers by which TORC1 may control autophagic processes other than phosphorylating Atg13 (Kamada et al., 2000). Of note, we also identified four potential TORC1 sites on Atg1, in agreement with data obtained on mammalian ULK1 (Hosokawa et al., 2009; Jung et al., 2009; Kim et al., 2011).

Analysis of the Atg1-dependent phosphoproteome revealed a similarly complex network of interactions specifically with the TORC1 signaling branch. For instance, Atg1 may feedback regulate TORC1 by (directly or indirectly) (1) impinging on Seh1 and Sea4, two subunits of the SEACAT complex that controls TORC1 through the Rag GTPases (Panchaud et al., 2013); (2) regulating Ser^{327} phosphorylation within the TORC1 subunit

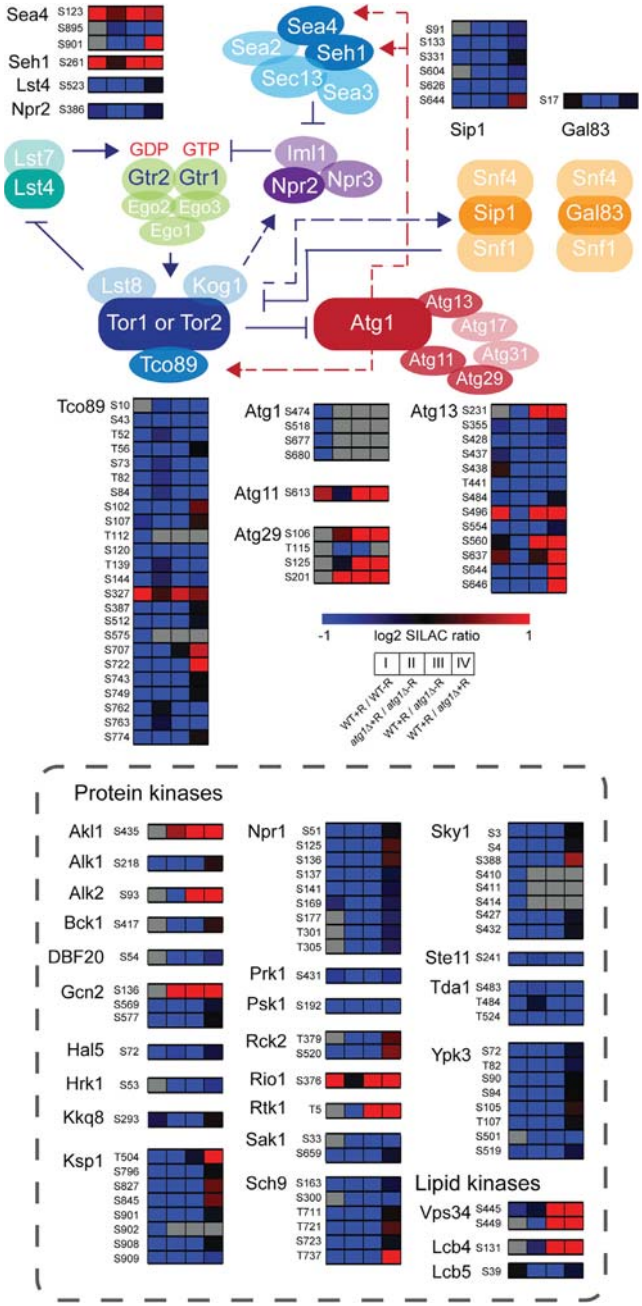

Figure 3. Kinases Carrying Rapamycin-Sensitive Phosphosites

Proteins carrying significantly regulated phosphosites were screened for kinases and known members of TORC1 and Atg1 signaling pathways. Potential TORC1 sites have a negative log2 SILAC ratio and are colored blue, and potential Atg1 sites have a positive log2 SILAC ratio and are colored red. If sites were not detected in specific experiments, their boxes are colored gray. Sites may be either activating or inhibiting. It is assumed that TORC1 and Atg1 have opposing effects on targets (i.e., act either activating or inhibiting). Solid lines indicate known interactions, and dashed lines indicate potential interactions identified in this study. Note: except Sky1 (n = 3), all kinases were quantified in a minimum of four replicates.

Tco89; and/or (3) controlling the Ser^{445}/Ser^{449} phosphorylation within the PI3-kinase Vps34 that is key for TORC1 and autophagy activation (Reidick et al., 2017; Tanigawa and Maeda, 2017) (Figure 3). Lastly, Atg1 also converges with TORC1 on Gcn2. Thus, Atg1 signaling seems to be much more intimately connected to TORC1 signaling than previously anticipated. Not surprisingly, this close relationship also extends to include the Snf1/AMPK complex, a major energy sensor and negative regulator of TORC1 in eukaryotic cells (Figure 3) (Hughes Hallett et al., 2015). Accordingly, TORC1 may feedback regulate Snf1 by controlling the phosphorylation state of various residues in the Snf1-activating protein kinase Sak1 and the Snf1 complex β-subunits Sip1 and Gal83 (Elbing et al., 2006; Schmidt and McCartney, 2000).

TORC1 and Atg1 Regulate Autophagy on Multiple Layers

Our SILAC-based screen indicated that Atg2, Atg9, Atg13, Atg26, and Atg29 carried both potential TORC1 and Atg1 target residues (Figure 4A). Using a phospho-specific antibody that recognizes pSer554 on Atg13, we corroborated in one case that a potential TORC1 target residue is indeed rapidly dephosphorylated in rapamycin-treated cells (Figure 4B). To test if any of the identified phosphorylation events were bona fide TORC1 or Atg1 sites, we then purified the 36 Atg proteins of yeast that are known to be involved in canonical autophagy (Wen and Klionsky, 2016) and performed TORC1 and Atg1 *in vitro* kinase assays coupled to quantitative MS as readout (Figure 4C) (Hatakeyama et al., 2019; Péli-Gulli et al., 2017). Proteins were purified from tandem affinity purification (TAP)- and glutathione S-transferase (GST)-tagged yeast collections (Gelperin et al., 2005; Zhu et al., 2000) and kinase assays in combination with MS sample processing were performed on molecular-weight cutoff filters using $^{18}O_4$-labeled ATP to separate *in vitro* from remnant *in vivo* phosphorylation events (Figure 4D) (Xue et al., 2014; Zhou et al., 2007). To identify direct phosphorylation events of Atg1 and TORC1, we performed label-free quantitative proteomics experiments comparing kinase assays with Atg1^{WT} to the ones with Atg1$^{kinase\ dead}$, and kinase assays with TORC1 with or without wortmannin (n = 3; Table S4), a PI3K inhibitor that potently inhibits TORC1 (Brunn et al., 1996; Urban et al., 2007). Of note, background phosphorylation levels were similar for all Atg substrates, and we did not identify elevated phosphorylation levels of Atg1 complex members. The respective data covered 139 out of 182 phosphosites on both Atg proteins and TORC1 subunits that are reported in the *Saccharomyces* Genome Database (76%; https://www.yeastgenome.org/). Notably, we further identified 406 hitherto unknown sites, indicating that our dataset includes and significantly expands the known, potentially biologically relevant target sites of Atg1 and TORC1 on Atg proteins. *In vitro* analyses confirmed the Atg1 motif generated using *in vivo* data (Figure 4E). The inferred *in vivo* and *in vitro* TORC1 motifs, however, differed substantially, which indicates that many of the rapamycin-sensitive phosphosites might be regulated indirectly by TORC1 effector kinases, such as Sch9 (Figure 2D), or protein phosphatases, such as Ptc2/3, that remove inhibitory TORC1 phosphosites from the Atg1-Atg13 complex (Memisoglu et al., 2019). From the *in vitro* data, we conclude that TORC1 phosphorylates preferentially serine residues that are followed

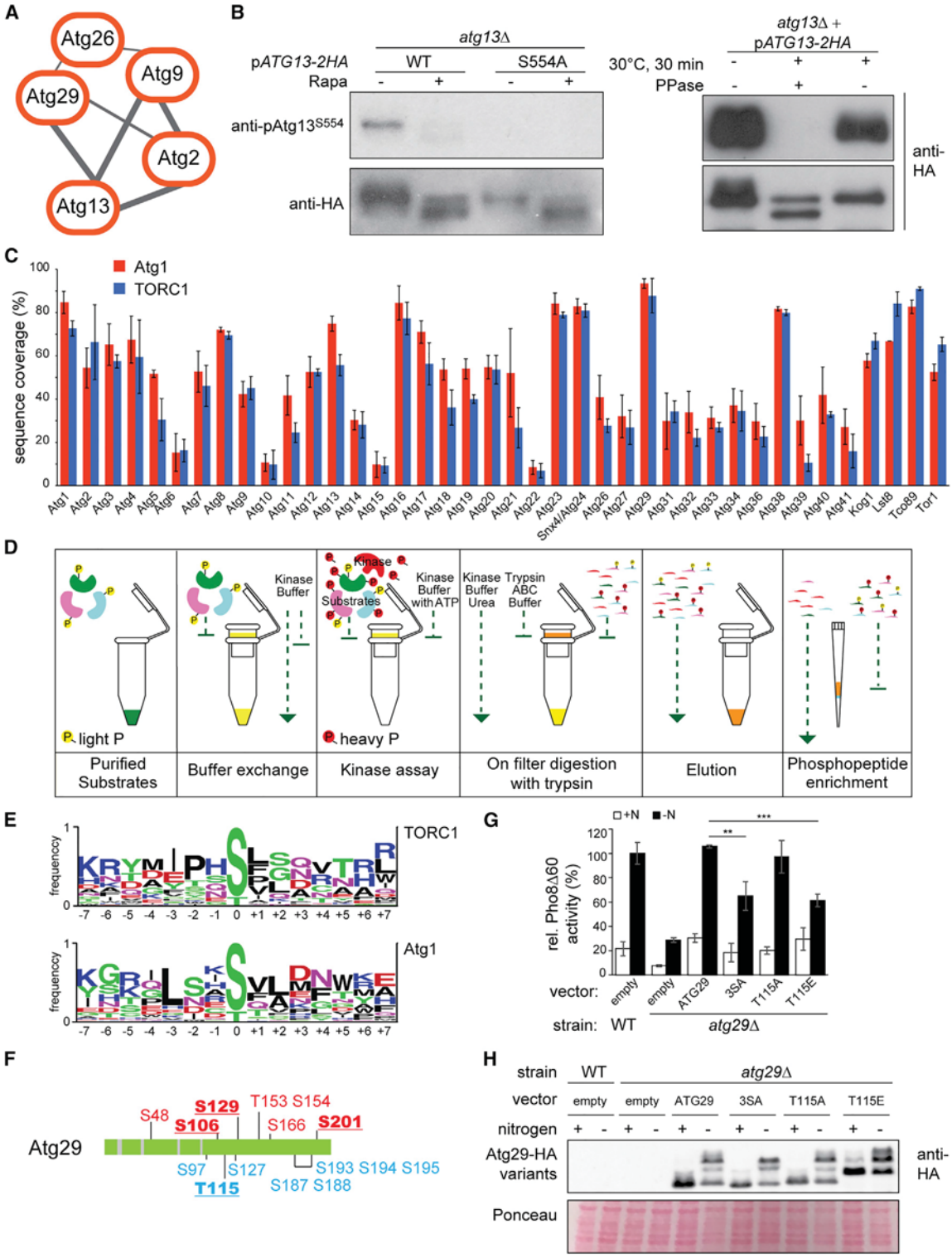

Figure 4. Filter-Aided *In Vitro* Kinase Assay to Identify Direct TORC1 and Atg1 Substrates

(A) Atg protein network carrying potential *in vivo* Atg1 and TORC1 sites generated by STRING database (DB). The thickness of connections indicates the strength of data support.

(B) Immunoblot analysis highlighting that Atg13 is phosphorylated by TORC1 on S554. A custom-made, site-specific antibody recognizing the phosphorylation of S554 on Atg13 and an anti-hemagglutinin (HA) antibody were used.

(legend continued on next page)

by hydrophobic residues in position +1. *In vitro* kinase assays appear, therefore, to be a valuable tool to corroborate direct TORC1 targets within the Atg protein network (Kang et al., 2013).

We identified phosphosites on 20 of the 36 purified Atg proteins, several of them being conserved in higher organisms (Figures S2 and S3; Table S4). By combining *in vivo* and *in vitro* analyses, it became evident that Atg1 and TORC1 likely regulate autophagy on multiple layers. So far, it was thought that TORC1 regulates solely the initiation of autophagy by phosphorylating Atg13. Our data, however, reveal additional TORC1 sites on Atg1, Atg2, Atg9, and Atg29 (Figures 4F and S2). Whereas Atg29 is also part of the Atg1 complex regulating the signal initiation, Atg2 and Atg9 take part in downstream processes that are critical for phagophore nucleation and expansion (Wen and Klionsky, 2016). The role of Atg1 appeared even more intertwined with the rest of the Atg machinery. It phosphorylated Atg2, Atg9, Atg12, Atg13, Atg23, and Atg29 (Figures 4F and S2), having potential implications in multiple steps of autophagosome biogenesis (Wen and Klionsky, 2016). Thus, TORC1 and Atg1 signaling appeared closely interconnected, phosphorylating multiple members of the Atg protein network, which may allow robust and coordinated control of autophagy initiation.

To test for biological relevance of the newly identified phosphosites, we analyzed their effects on autophagy using the Pho8Δ60 assay as described (Noda et al., 1995). We focused on the Atg1 complex member Atg29 and generated an *atg29*Δ strain, which displayed a significant block in autophagy activity under nitrogen starvation conditions (Figures 4G and 4H). In agreement with published data, serine-to-alanine mutations of Atg1 target sites Ser197, Ser199, and Ser201 (3SA) significantly reduced autophagy (Figures 4G and S3A; $p < 0.01$) (Mao et al., 2013). Importantly, a single phospho-mimicking threonine-to-glutamate mutation of the newly identified TORC1 target site Thr115 (T115E) also significantly decreased autophagic activity under starvation conditions, whereas a threonine-to-alanine mutation (T115A) had no effect (Figure 4G; $p < 0.001$). Thus, Atg29 integrates both Atg1 and TORC1 signaling *in vivo* to properly regulate autophagy.

DISCUSSION

In this study, we comprehensively characterized signaling events regulated by two conserved kinase complexes—the TORC1 and its downstream effector Atg1—critical for cell homeostasis during nutrient deprivation. Moreover, we identified a multilayered control of autophagy by TORC1 and Atg1 signaling, including negative and positive feedback loops, by generating the currently most comprehensive dataset of rapamycin-sensitive, phosphorylation-based signaling events in the budding yeast *S. cerevisiae*, covering 36,600 phosphorylation sites and over 80% of the technically detectable phosphorylated residues. Compared to published reports, our data corroborate, on average, 12% of the reported rapamycin-sensitive sites, which highlights the experimental and biological noise of phosphoproteomics studies. To address this challenge, we decided to perform five biological replicates and to stringently filter the reported regulated sites using a random effect model.

The question if specific sites are direct kinase targets or if the observed effects are of secondary nature conveyed by downstream effector kinases is not easy to address. The kinetic analysis of *in vivo* events may shed light onto primary and secondary events (Oliveira et al., 2015; Rigbolt et al., 2014). However, the gold standard for proving direct kinase-substrate interactions is still classical *in vitro* kinase assays. Therefore, we purified 36 yeast Atg proteins that are involved in starvation-induced autophagy and used them as substrates in *in vitro* protein kinase assays (Wen and Klionsky, 2016). Notably, we filtered the *in vitro* data with *in vivo* recordings to eliminate non-physiological phosphorylation events *in vitro* (e.g., due to missing binding partners or cellular compartmentalization). Thus, the sites shortlisted are likely to correspond to bona fide TORC1 or Atg1 sites.

Within the set of protein kinases exhibiting potential TORC1 sites, we identified several that have previously been linked to autophagic processes: (1) Bck1 mediates signals from Pkc1 to Mkk1/2 within the cell wall integrity MAPK signaling pathway (Krause and Gray, 2002), which is required for the induction of pexophagy in yeast (Manjithaya et al., 2010); (2) Ksp1 inhibits autophagy by antagonizing the dephosphorylation of Atg13 (Umekawa and Klionsky, 2012); and (3) Sky1 modulates mitophagy (Rodríguez-Lombardero et al., 2014). Shared signaling events between organelle-specific autophagy subtypes and bulk autophagy might indicate that selective autophagy contributes to the bulk protein turnover observed in nutrient-starvation conditions. Supporting this hypothesis, we identified regulated phosphosites on Cue5, a ubiquitin-Atg8 receptor involved in the selective degradation of polyQ proteins (Lu et al., 2014), on the ubiquitin protease Ubp3/Bre5 as being critical for ribophagy

(C) Sequence mapping of proteins used in *in vitro* kinase assays. Sequence coverage of Atg proteins purified from GST- and TAP-tagged yeast strains is shown. Trypsin was used as protease for bottom-up proteomics experiments. Error bars indicate standard deviations (n = 3).
(D) Workflow of the filter-aided *in vitro* kinase assay. Phosphopeptides enriched by TiO_2 chromatography are analyzed by LC-MS/MS.
(E) Sequence motifs of phosphosites enriched in TORC1 and Atg1 *in vitro* kinase assays.
(F) Graphic representation of purified Atg29 used in *in vitro* kinase assays. *In vitro* TORC1 sites are annotated in blue and Atg1 sites in red. Sites that are underlined and marked in bold were identified by *in vivo* and *in vitro* assays. Protein sequences covered by MS analyses are marked in green.
(G) Cells (*pho8Δ60* labeled with WT; *pho8Δ60 atg29Δ* labeled with *atg29Δ*) were transformed with an empty vector (empty) or vectors encoding the indicated HA-tagged Atg29 variants. Cells were grown exponentially for 24 h in SD (+N) and then shifted to SD-N for 3 h (–N). Protein extracts were analyzed by ALP assay. Error bars were obtained from at least three independent repeats and indicate SDs. Pho8Δ60 phosphatase activities were normalized to the ones of nitrogen-starved WT cells (100%). $^{**}p < 0.01$; $^{***}p < 0.001$, t test.
(H) In parallel, protein extracts were also subjected to immunoblot analysis (using anti-HA antibodies) to assess the appropriate expression of the HA-tagged Atg29 variants (upper part of the panel). Ponceau staining served as loading controls (lower part). Note that the altered migration pattern of Atg29-T115E is likely caused by an altered charge state of the protein due to the introduction of an acidic amino acid.
See also Figures S2 and S3.

(Kraft et al., 2008) and on Nvj1 and Vac8, which cooperate in piecemeal microautophagy of the nucleus (Roberts et al., 2003) (Table S1). Importantly, we characterized Atg1, Atg2, Atg9, and Atg29 as potential new direct TORC1 targets within the Atg machinery. Thus, similar to the situation in mammalian cells where ULK1 itself was identified as an mTORC1 target (Hosokawa et al., 2009; Jung et al., 2009), we identified one phosphosite (Ser518) on Atg1 as a potential direct TORC1 site. Interestingly, of the three additional sites that were identified as negatively regulated by rapamycin treatment *in vivo,* only Ser677 and Ser680 lie within the EAT/tMIT domain, which is critical for Atg13 binding (Fujioka et al., 2014; Ragusa et al., 2012). Thus, TORC1 may directly influence Atg1-Atg13 activity by phosphorylating both complex members. In addition, TORC1 seems to also negatively regulate the second subcomplex of the Atg1 holo-complex, Atg17-Atg31-Atg29, by phosphorylating Thr115 of Atg29.

Next to TORC1 target sites, we also characterized 162 potential Atg1 sites on 128 proteins. Our data confirmed phosphorylations on Atg2 (Ser249) and Atg9 (Ser802 and Ser969) (Papinski et al., 2014), but the majority of the identified sites are so far unknown and need future investigations to understand their significance in autophagy and beyond. Within the Atg protein network, we identified new bona fide Atg1 sites on Atg2, Atg9, Atg13, Atg23, Atg29, and Atg33, an outer mitochondrial membrane protein involved in mitophagy (Kanki et al., 2009). It appears that Atg1 is not only critical for autophagy initiation, but it also controls the entire pathway, including organelle-specific autophagy subtypes as well as autophagosome-vacuole fusion, by phosphorylating the SNARE proteins Vti1 and Ykt6 (Table S1) (Bas et al., 2018; Gao et al., 2018). Importantly, Atg1 seems to not only receive input from TORC1, but also regulate TORC1 activity by phosphorylating members of the SEACAT complex, an activator of TORC1, which inhibits SEACIT, a GTPase-activating protein (GAP) of Gtr1. Whether Atg1 phosphorylation of SEACAT acts positively or negatively on TORC1 activity will have to be addressed in future studies. Nevertheless, the functions of Atg1 seem to be broader than anticipated, potentially controlling cell homeostasis by phosphorylating target proteins outside of the canonical Atg protein network. In summary, our study uncovers a multilayered signaling network, which serves to coordinate TORC1 and Atg1 activities to robustly tune autophagy in response to nutritional cues, and it lays the groundwork for future mechanistic approaches.

STAR★METHODS

Detailed methods are provided in the online version of this paper and include the following:

- KEY RESOURCES TABLE
- LEAD CONTACT AND MATERIALS AVAILABILITY
- EXPERIMENTAL MODEL AND SUBJECT DETAILS
  - Yeast strains, plasmids, and growth conditions
  - Sample preparation of *in vivo* SILAC experiments
- METHOD DETAILS
  - Filter-Aided *In Vitro* Kinase Assay
  - Phosphopeptide Enrichment
  - LC-MS/MS Analyses
  - ALP assays for the determination of autophagic flux and immunoblot analysis
- QUANTIFICATION AND STATISTICAL ANALYSIS
- DATA AND CODE AVAILABILITY

SUPPLEMENTAL INFORMATION

Supplemental Information can be found online at https://doi.org/10.1016/j.celrep.2019.08.069.

ACKNOWLEDGMENTS

This research was generously supported by the Canton of Fribourg and the Swiss National Science Foundation (J.D., C.D.V., and R.R.) and by TRANSAUTOPHAGY, COST Action CA15138 (J.D. and F.R.). F.R. is supported by ZonMW VICI (016.130.606), ZonMW TOP (91217002), ALW Open Programme (ALWOP.310), Marie Skłodowska-Curie Cofund (713660), and Marie Skłodowska Curie ETN (765912) grants.

AUTHOR CONTRIBUTIONS

Conceptualization, C.D.V. and J.D.; Methodology, Z.H., S.R., M.J., R.H., M.S., R.R., F.R., C.D.V., and J.D.; Investigation, Z.H., S.R., M.J., R.H., M.S., R.R., and F.R.; Writing - Original Draft, C.D.V. and J.D.; Writing - Review & Editing, Z.H., R.R., F.R., C.D.V., and J.D.; Funding Acquisition, Resources, & Supervision, F.R., C.D.V., and J.D.

DECLARATION OF INTERESTS

The authors declare no competing interests.

Received: May 7, 2019
Revised: July 19, 2019
Accepted: August 22, 2019
Published: September 24, 2019

SUPPORTING CITATIONS

The following references appear in the Supplemental Information: Bertram et al. (2000); Boeckstaens et al. (2014); Boeckstaens et al. (2015); Bontron et al. (2013); Breslow and Weissman (2010); Dever et al. (1992); Feng et al. (2016); Gander et al. (2008); Huber et al. (2011); Lee et al. (2009); MacGurn et al. (2011); Martín et al. (2011); Moreno-Torres et al. (2015); O'Donnell et al. (2010); Sánchez-Wandelmer et al. (2017); Shimobayashi et al. (2013); Talarek et al. (2010); Varlakhanova et al. (2018); Wanke et al. (2005); Wanke et al. (2008); Yeh et al. (2010).

REFERENCES

Albert, V., and Hall, M.N. (2015). mTOR signaling in cellular and organismal energetics. Curr. Opin. Cell Biol. *33*, 55–66.

Azeloglu, E.U., and Iyengar, R. (2015). Signaling networks: information flow, computation, and decision making. Cold Spring Harb. Perspect. Biol. *7*, a005934.

Bas, L., Papinski, D., Licheva, M., Torggler, R., Rohringer, S., Schuschnig, M., and Kraft, C. (2018). Reconstitution reveals Ykt6 as the autophagosomal SNARE in autophagosome-vacuole fusion. J. Cell Biol. *217*, 3656–3669.

Bates, D., Mächler, M., Bolker, B., and Walker, S. (2015). Fitting linear mixed-effects models using lme4. J. Stat. Softw. *67*.

Batth, T.S., Francavilla, C., and Olsen, J.V. (2014). Off-line high-pH reversed-phase fractionation for in-depth phosphoproteomics. J. Proteome Res. *13*, 6176–6186.

Batth, T.S., Papetti, M., Pfeiffer, A., Tollenaere, M.A.X., Francavilla, C., and Olsen, J.V. (2018). Large-Scale Phosphoproteomics reveals Shp-2

phosphatase-dependent regulators of Pdgf receptor signaling. Cell Rep. *22*, 2784–2796.

Bentley, M., and Banker, G. (2015). A novel assay to identify the trafficking proteins that bind to specific vesicle populations. Curr. Protoc. Cell Biol. *69*, 13.8.1–13.8.12.

Bertram, P.G., Choi, J.H., Carvalho, J., Ai, W., Zeng, C., Chan, T.F., and Zheng, X.F. (2000). Tripartite regulation of Gln3p by TOR, Ure2p, and phosphatases. J. Biol. Chem. *275*, 35727–35733.

Bindea, G., Mlecnik, B., Hackl, H., Charoentong, P., Tosolini, M., Kirilovsky, A., Fridman, W.H., Pagès, F., Trajanoski, Z., and Galon, J. (2009). ClueGO: a Cytoscape plug-in to decipher functionally grouped gene ontology and pathway annotation networks. Bioinformatics *25*, 1091–1093.

Boeckstaens, M., Llinares, E., Van Vooren, P., and Marini, A.M. (2014). The TORC1 effector kinase Npr1 fine tunes the inherent activity of the Mep2 ammonium transport protein. Nat. Commun. *5*, 3101.

Boeckstaens, M., Merhi, A., Llinares, E., Van Vooren, P., Springael, J.Y., Wintjens, R., and Marini, A.M. (2015). Identification of a Novel Regulatory Mechanism of Nutrient Transport Controlled by TORC1-Npr1-Amu1/Par32. PLoS Genet. *11*, e1005382.

Bontron, S., Jaquenoud, M., Vaga, S., Talarek, N., Bodenmiller, B., Aebersold, R., and De Virgilio, C. (2013). Yeast endosulfines control entry into quiescence and chronological life span by inhibiting protein phosphatase 2A. Cell Rep. *3*, 16–22.

Breitkreutz, A., Choi, H., Sharom, J.R., Boucher, L., Neduva, V., Larsen, B., Lin, Z.Y., Breitkreutz, B.J., Stark, C., Liu, G., et al. (2010). A global protein kinase and phosphatase interaction network in yeast. Science *328*, 1043–1046.

Breslow, D.K., and Weissman, J.S. (2010). Membranes in balance: mechanisms of sphingolipid homeostasis. Mol. Cell *40*, 267–279.

Brunn, G.J., Williams, J., Sabers, C., Wiederrecht, G., Lawrence, J.C., Jr., and Abraham, R.T. (1996). Direct inhibition of the signaling functions of the mammalian target of rapamycin by the phosphoinositide 3-kinase inhibitors, wortmannin and LY294002. EMBO J. *15*, 5256–5267.

Cherkasova, V.A., and Hinnebusch, A.G. (2003). Translational control by TOR and TAP42 through dephosphorylation of eIF2α kinase GCN2. Genes Dev. *17*, 859–872.

Corcoles-Saez, I., Dong, K., Johnson, A.L., Waskiewicz, E., Costanzo, M., Boone, C., and Cha, R.S. (2018). Essential Function of Mec1, the Budding Yeast ATM/ATR Checkpoint-Response Kinase, in Protein Homeostasis. Dev. Cell *46*, 495–503.e492.

Cox, J., and Mann, M. (2008). MaxQuant enables high peptide identification rates, individualized p.p.b.-range mass accuracies and proteome-wide protein quantification. Nat. Biotechnol. *26*, 1367–1372.

Dever, T.E., Feng, L., Wek, R.C., Cigan, A.M., Donahue, T.F., and Hinnebusch, A.G. (1992). Phosphorylation of initiation factor 2α by protein kinase GCN2 mediates gene-specific translational control of *GCN4* in yeast. Cell *68*, 585–596.

Dikic, I., and Elazar, Z. (2018). Mechanism and medical implications of mammalian autophagy. Nat. Rev. Mol. Cell Biol. *19*, 349–364.

Eapen, V.V., Waterman, D.P., Bernard, A., Schiffmann, N., Sayas, E., Kamber, R., Lemos, B., Memisoglu, G., Ang, J., Mazella, A., et al. (2017). A pathway of targeted autophagy is induced by DNA damage in budding yeast. Proc. Natl. Acad. Sci. USA *114*, E1158–E1167.

Egan, D.F., Chun, M.G., Vamos, M., Zou, H., Rong, J., Miller, C.J., Lou, H.J., Raveendra-Panickar, D., Yang, C.C., Sheffler, D.J., et al. (2015). Small Molecule Inhibition of the Autophagy Kinase ULK1 and Identification of ULK1 Substrates. Mol. Cell *59*, 285–297.

Elbing, K., McCartney, R.R., and Schmidt, M.C. (2006). Purification and characterization of the three Snf1-activating kinases of *Saccharomyces cerevisiae*. Biochem. J. *393*, 797–805.

Feng, Y., Backues, S.K., Baba, M., Heo, J.M., Harper, J.W., and Klionsky, D.J. (2016). Phosphorylation of Atg9 regulates movement to the phagophore assembly site and the rate of autophagosome formation. Autophagy *12*, 648–658.

Fujioka, Y., Suzuki, S.W., Yamamoto, H., Kondo-Kakuta, C., Kimura, Y., Hirano, H., Akada, R., Inagaki, F., Ohsumi, Y., and Noda, N.N. (2014). Structural basis of starvation-induced assembly of the autophagy initiation complex. Nat. Struct. Mol. Biol. *21*, 513–521.

Gander, S., Bonenfant, D., Altermatt, P., Martin, D.E., Hauri, S., Moes, S., Hall, M.N., and Jenoe, P. (2008). Identification of the rapamycin-sensitive phosphorylation sites within the Ser/Thr-rich domain of the yeast Npr1 protein kinase. Rapid Commun. Mass Spectrom. *22*, 3743–3753.

Gao, J., Reggiori, F., and Ungermann, C. (2018). A novel in vitro assay reveals SNARE topology and the role of Ykt6 in autophagosome fusion with vacuoles. J. Cell Biol. *217*, 3670–3682.

Garcia-Barrio, M., Dong, J., Cherkasova, V.A., Zhang, X., Zhang, F., Ufano, S., Lai, R., Qin, J., and Hinnebusch, A.G. (2002). Serine 577 is phosphorylated and negatively affects the tRNA binding and eIF2α kinase activities of GCN2. J. Biol. Chem. *277*, 30675–30683.

Gelperin, D.M., White, M.A., Wilkinson, M.L., Kon, Y., Kung, L.A., Wise, K.J., Lopez-Hoyo, N., Jiang, L., Piccirillo, S., Yu, H., et al. (2005). Biochemical and genetic analysis of the yeast proteome with a movable ORF collection. Genes Dev. *19*, 2816–2826.

González, A., Shimobayashi, M., Eisenberg, T., Merle, D.A., Pendl, T., Hall, M.N., and Moustafa, T. (2015). TORC1 promotes phosphorylation of ribosomal protein S6 via the AGC kinase Ypk3 in *Saccharomyces cerevisiae*. PLoS ONE *10*, e0120250.

Harding, M.W., Galat, A., Uehling, D.E., and Schreiber, S.L. (1989). A receptor for the immunosuppressant FK506 is a cis-trans peptidyl-prolyl isomerase. Nature *341*, 758–760.

Hatakeyama, R., Péli-Gulli, M.P., Hu, Z., Jaquenoud, M., Garcia Osuna, G.M., Sardu, A., Dengjel, J., and De Virgilio, C. (2019). Spatially Distinct Pools of TORC1 Balance Protein Homeostasis. Mol. Cell *73*, 325–338.e328.

Heitman, J., Movva, N.R., and Hall, M.N. (1991). Targets for cell cycle arrest by the immunosuppressant rapamycin in yeast. Science *253*, 905–909.

Horn, H., Schoof, E.M., Kim, J., Robin, X., Miller, M.L., Diella, F., Palma, A., Cesareni, G., Jensen, L.J., and Linding, R. (2014). KinomeXplorer: an integrated platform for kinome biology studies. Nat. Methods *11*, 603–604.

Hosokawa, N., Hara, T., Kaizuka, T., Kishi, C., Takamura, A., Miura, Y., Iemura, S., Natsume, T., Takehana, K., Yamada, N., et al. (2009). Nutrient-dependent mTORC1 association with the ULK1-Atg13-FIP200 complex required for autophagy. Mol. Biol. Cell *20*, 1981–1991.

Huber, A., Bodenmiller, B., Uotila, A., Stahl, M., Wanka, S., Gerrits, B., Aebersold, R., and Loewith, R. (2009). Characterization of the rapamycin-sensitive phosphoproteome reveals that Sch9 is a central coordinator of protein synthesis. Genes Dev. *23*, 1929–1943.

Huber, A., French, S.L., Tekotte, H., Yerlikaya, S., Stahl, M., Perepelkina, M.P., Tyers, M., Rougemont, J., Beyer, A.L., and Loewith, R. (2011). Sch9 regulates ribosome biogenesis via Stb3, Dot6 and Tod6 and the histone deacetylase complex RPD3L. EMBO J. *30*, 3052–3064.

Hughes Hallett, J.E., Luo, X., and Capaldi, A.P. (2015). Snf1/AMPK promotes the formation of Kog1/Raptor-bodies to increase the activation threshold of TORC1 in budding yeast. eLife *4*, e09181.

Hurley, J.H., and Young, L.N. (2017). Mechanisms of Autophagy Initiation. Annu. Rev. Biochem. *86*, 225–244.

Iesmantavicius, V., Weinert, B.T., and Choudhary, C. (2014). Convergence of ubiquitylation and phosphorylation signaling in rapamycin-treated yeast cells. Mol. Cell. Proteomics *13*, 1979–1992.

Jung, C.H., Jun, C.B., Ro, S.H., Kim, Y.M., Otto, N.M., Cao, J., Kundu, M., and Kim, D.H. (2009). ULK-Atg13-FIP200 complexes mediate mTOR signaling to the autophagy machinery. Mol. Biol. Cell *20*, 1992–2003.

Kamada, Y., Funakoshi, T., Shintani, T., Nagano, K., Ohsumi, M., and Ohsumi, Y. (2000). Tor-mediated induction of autophagy via an Apg1 protein kinase complex. J. Cell Biol. *150*, 1507–1513.

Kamada, Y., Yoshino, K., Kondo, C., Kawamata, T., Oshiro, N., Yonezawa, K., and Ohsumi, Y. (2010). Tor directly controls the Atg1 kinase complex to regulate autophagy. Mol. Cell. Biol. *30*, 1049–1058.

Kang, S.A., Pacold, M.E., Cervantes, C.L., Lim, D., Lou, H.J., Ottina, K., Gray, N.S., Turk, B.E., Yaffe, M.B., and Sabatini, D.M. (2013). mTORC1 phosphorylation sites encode their sensitivity to starvation and rapamycin. Science *341*, 1236566.

Kanki, T., Wang, K., Baba, M., Bartholomew, C.R., Lynch-Day, M.A., Du, Z., Geng, J., Mao, K., Yang, Z., Yen, W.L., and Klionsky, D.J. (2009). A genomic screen for yeast mutants defective in selective mitochondria autophagy. Mol. Biol. Cell *20*, 4730–4738.

Kawamata, T., Kamada, Y., Kabeya, Y., Sekito, T., and Ohsumi, Y. (2008). Organization of the pre-autophagosomal structure responsible for autophagosome formation. Mol. Biol. Cell *19*, 2039–2050.

Kim, J., Kundu, M., Viollet, B., and Guan, K.L. (2011). AMPK and mTOR regulate autophagy through direct phosphorylation of Ulk1. Nat. Cell Biol. *13*, 132–141.

Klionsky, D.J., Baehrecke, E.H., Brumell, J.H., Chu, C.T., Codogno, P., Cuervo, A.M., Debnath, J., Deretic, V., Elazar, Z., Eskelinen, E.L., et al. (2011). A comprehensive glossary of autophagy-related molecules and processes (2nd edition). Autophagy *7*, 1273–1294.

Klionsky, D.J., Abdelmohsen, K., Abe, A., Abedin, M.J., Abeliovich, H., Acevedo Arozena, A., Adachi, H., Adams, C.M., Adams, P.D., Adeli, K., et al. (2016). Guidelines for the use and interpretation of assays for monitoring autophagy (3rd edition). Autophagy *12*, 1–222.

Kraft, C., Deplazes, A., Sohrmann, M., and Peter, M. (2008). Mature ribosomes are selectively degraded upon starvation by an autophagy pathway requiring the Ubp3p/Bre5p ubiquitin protease. Nat. Cell Biol. *10*, 602–610.

Krause, S.A., and Gray, J.V. (2002). The protein kinase C pathway is required for viability in quiescence in *Saccharomyces cerevisiae*. Curr. Biol. *12*, 588–593.

Lee, J., Moir, R.D., and Willis, I.M. (2009). Regulation of RNA polymerase III transcription involves SCH9-dependent and SCH9-independent branches of the target of rapamycin (TOR) pathway. J. Biol. Chem. *284*, 12604–12608.

Lempiäinen, H., Uotila, A., Urban, J., Dohnal, I., Ammerer, G., Loewith, R., and Shore, D. (2009). Sfp1 interaction with TORC1 and Mrs6 reveals feedback regulation on TOR signaling. Mol. Cell *33*, 704–716.

Lu, K., Psakhye, I., and Jentsch, S. (2014). Autophagic clearance of polyQ proteins mediated by ubiquitin-Atg8 adaptors of the conserved CUET protein family. Cell *158*, 549–563.

MacGurn, J.A., Hsu, P.C., Smolka, M.B., and Emr, S.D. (2011). TORC1 regulates endocytosis via Npr1-mediated phosphoinhibition of a ubiquitin ligase adaptor. Cell *147*, 1104–1117.

Madeira, F., Park, Y.M., Lee, J., Buso, N., Gur, T., Madhusoodanan, N., Basutkar, P., Tivey, A.R.N., Potter, S.C., Finn, R.D., and Lopez, R. (2019). The EMBL-EBI search and sequence analysis tools APIs in 2019. Nucleic Acids Res. *47* (*W1*), W636–W641.

Manjithaya, R., Jain, S., Farré, J.C., and Subramani, S. (2010). A yeast MAPK cascade regulates pexophagy but not other autophagy pathways. J. Cell Biol. *189*, 303–310.

Mao, K., Chew, L.H., Inoue-Aono, Y., Cheong, H., Nair, U., Popelka, H., Yip, C.K., and Klionsky, D.J. (2013). Atg29 phosphorylation regulates coordination of the Atg17-Atg31-Atg29 complex with the Atg11 scaffold during autophagy initiation. Proc. Natl. Acad. Sci. USA *110*, E2875–E2884.

Martin, D.E., Soulard, A., and Hall, M.N. (2004). TOR regulates ribosomal protein gene expression via PKA and the Forkhead transcription factor FHL1. Cell *119*, 969–979.

Martín, Y., González, Y.V., Cabrera, E., Rodríguez, C., and Siverio, J.M. (2011). Npr1 Ser/Thr protein kinase links nitrogen source quality and carbon availability with the yeast nitrate transporter (Ynt1) levels. J. Biol. Chem. *286*, 27225–27235.

Memisoglu, G., Eapen, V.V., Yang, Y., Klionsky, D.J., and Haber, J.E. (2019). PP2C phosphatases promote autophagy by dephosphorylation of the Atg1 complex. Proc. Natl. Acad. Sci. USA *116*, 1613–1620.

Mizushima, N., Yoshimori, T., and Ohsumi, Y. (2011). The role of Atg proteins in autophagosome formation. Annu. Rev. Cell Dev. Biol. *27*, 107–132.

Mok, J., Kim, P.M., Lam, H.Y., Piccirillo, S., Zhou, X., Jeschke, G.R., Sheridan, D.L., Parker, S.A., Desai, V., Jwa, M., et al. (2010). Deciphering protein kinase specificity through large-scale analysis of yeast phosphorylation site motifs. Sci. Signal. *3*, ra12.

Moreno-Torres, M., Jaquenoud, M., and De Virgilio, C. (2015). TORC1 controls G_1-S cell cycle transition in yeast via Mpk1 and the greatwall kinase pathway. Nat. Commun. *6*, 8256.

Noda, T., Matsuura, A., Wada, Y., and Ohsumi, Y. (1995). Novel system for monitoring autophagy in the yeast *Saccharomyces cerevisiae*. Biochem. Biophys. Res. Commun. *210*, 126–132.

O'Donnell, A.F., Apffel, A., Gardner, R.G., and Cyert, M.S. (2010). α-arrestins Aly1 and Aly2 regulate intracellular trafficking in response to nutrient signaling. Mol. Biol. Cell *21*, 3552–3566.

Oliveira, A.P., Ludwig, C., Zampieri, M., Weisser, H., Aebersold, R., and Sauer, U. (2015). Dynamic phosphoproteomics reveals TORC1-dependent regulation of yeast nucleotide and amino acid biosynthesis. Sci. Signal. *8*, rs4.

Olsen, J.V., Blagoev, B., Gnad, F., Macek, B., Kumar, C., Mortensen, P., and Mann, M. (2006). Global, in vivo, and site-specific phosphorylation dynamics in signaling networks. Cell *127*, 635–648.

Panchaud, N., Péli-Gulli, M.P., and De Virgilio, C. (2013). SEACing the GAP that nEGOCiates TORC1 activation: evolutionary conservation of Rag GTPase regulation. Cell Cycle *12*, 2948–2952.

Papinski, D., Schuschnig, M., Reiter, W., Wilhelm, L., Barnes, C.A., Maiolica, A., Hansmann, I., Pfaffenwimmer, T., Kijanska, M., Stoffel, I., et al. (2014). Early steps in autophagy depend on direct phosphorylation of Atg9 by the Atg1 kinase. Mol. Cell *53*, 471–483.

Paulo, J.A., and Gygi, S.P. (2015). A comprehensive proteomic and phosphoproteomic analysis of yeast deletion mutants of 14-3-3 orthologs and associated effects of rapamycin. Proteomics *15*, 474–486.

Péli-Gulli, M.P., Raucci, S., Hu, Z., Dengjel, J., and De Virgilio, C. (2017). Feedback Inhibition of the Rag GTPase GAP Complex Lst4-Lst7 Safeguards TORC1 from Hyperactivation by Amino Acid Signals. Cell Rep. *20*, 281–288.

Perez-Riverol, Y., Csordas, A., Bai, J., Bernal-Llinares, M., Hewapathirana, S., Kundu, D.J., Inuganti, A., Griss, J., Mayer, G., Eisenacher, M., et al. (2019). The PRIDE database and related tools and resources in 2019: improving support for quantification data. Nucleic Acids Res. *47* (*D1*), D442–D450.

Ragusa, M.J., Stanley, R.E., and Hurley, J.H. (2012). Architecture of the Atg17 complex as a scaffold for autophagosome biogenesis. Cell *151*, 1501–1512.

Reidick, C., Boutouja, F., and Platta, H.W. (2017). The class III phosphatidylinositol 3-kinase Vps34 in *Saccharomyces cerevisiae*. Biol. Chem. *398*, 677–685.

Reinke, A., Anderson, S., McCaffery, J.M., Yates, J., 3rd, Aronova, S., Chu, S., Fairclough, S., Iverson, C., Wedaman, K.P., and Powers, T. (2004). TOR complex 1 includes a novel component, Tco89p (YPL180w), and cooperates with Ssd1p to maintain cellular integrity in *Saccharomyces cerevisiae*. J. Biol. Chem. *279*, 14752–14762.

Rigbolt, K.T., Zarei, M., Sprenger, A., Becker, A.C., Diedrich, B., Huang, X., Eiselein, S., Kristensen, A.R., Gretzmeier, C., Andersen, J.S., et al. (2014). Characterization of early autophagy signaling by quantitative phosphoproteomics. Autophagy *10*, 356–371.

Roberts, P., Moshitch-Moshkovitz, S., Kvam, E., O'Toole, E., Winey, M., and Goldfarb, D.S. (2003). Piecemeal microautophagy of nucleus in *Saccharomyces cerevisiae*. Mol. Biol. Cell *14*, 129–141.

Rodríguez-Lombardero, S., Rodríguez-Belmonte, M.E., González-Siso, M.I., Vizoso-Vázquez, Á., Valdiglesias, V., Laffón, B., and Cerdán, M.E. (2014). Proteomic analyses reveal that Sky1 modulates apoptosis and mitophagy in *Saccharomyces cerevisiae* cells exposed to cisplatin. Int. J. Mol. Sci. *15*, 12573–12590.

R Team. (2019). R: A language and environment for statistical computing (R Foundation for Statistical Computing).

Sánchez-Wandelmer, J., Kriegenburg, F., Rohringer, S., Schuschnig, M., Gómez-Sánchez, R., Zens, B., Abreu, S., Hardenberg, R., Hollenstein, D., Gao, J.,

et al. (2017). Atg4 proteolytic activity can be inhibited by Atg1 phosphorylation. Nat. Commun. *8*, 295.

Saxton, R.A., and Sabatini, D.M. (2017). mTOR Signaling in Growth, Metabolism, and Disease. Cell *168*, 960–976.

Schmelzle, T., Beck, T., Martin, D.E., and Hall, M.N. (2004). Activation of the RAS/cyclic AMP pathway suppresses a TOR deficiency in yeast. Mol. Cell. Biol. *24*, 338–351.

Schmidt, M.C., and McCartney, R.R. (2000). beta-subunits of Snf1 kinase are required for kinase function and substrate definition. EMBO J. *19*, 4936–4943.

Schmidt, A., Beck, T., Koller, A., Kunz, J., and Hall, M.N. (1998). The TOR nutrient signalling pathway phosphorylates NPR1 and inhibits turnover of the tryptophan permease. EMBO J. *17*, 6924–6931.

Shannon, P., Markiel, A., Ozier, O., Baliga, N.S., Wang, J.T., Ramage, D., Amin, N., Schwikowski, B., and Ideker, T. (2003). Cytoscape: a software environment for integrated models of biomolecular interaction networks. Genome Res. *13*, 2498–2504.

Shimobayashi, M., Oppliger, W., Moes, S., Jenö, P., and Hall, M.N. (2013). TORC1-regulated protein kinase Npr1 phosphorylates Orm to stimulate complex sphingolipid synthesis. Mol. Biol. Cell *24*, 870–881.

Sikorski, R.S., and Hieter, P. (1989). A system of shuttle vectors and yeast host strains designed for efficient manipulation of DNA in *Saccharomyces cerevisiae*. Genetics *122*, 19–27.

Soulard, A., Cremonesi, A., Moes, S., Schütz, F., Jenö, P., and Hall, M.N. (2010). The rapamycin-sensitive phosphoproteome reveals that TOR controls protein kinase A toward some but not all substrates. Mol. Biol. Cell *21*, 3475–3486.

Talarek, N., Cameroni, E., Jaquenoud, M., Luo, X., Bontron, S., Lippman, S., Devgan, G., Snyder, M., Broach, J.R., and De Virgilio, C. (2010). Initiation of the TORC1-regulated G_0 program requires Igo1/2, which license specific mRNAs to evade degradation via the 5′-3′ mRNA decay pathway. Mol. Cell *38*, 345–355.

Tanigawa, M., and Maeda, T. (2017). An *In Vitro* TORC1 Kinase Assay That Recapitulates the Gtr-Independent Glutamine-Responsive TORC1 Activation Mechanism on Yeast Vacuoles. Mol. Cell. Biol. *37*, e00075-17.

Tyanova, S., Temu, T., Sinitcyn, P., Carlson, A., Hein, M.Y., Geiger, T., Mann, M., and Cox, J. (2016). The Perseus computational platform for comprehensive analysis of (prote)omics data. Nat. Methods *13*, 731–740.

Umekawa, M., and Klionsky, D.J. (2012). Ksp1 kinase regulates autophagy via the target of rapamycin complex 1 (TORC1) pathway. J. Biol. Chem. *287*, 16300–16310.

Urban, J., Soulard, A., Huber, A., Lippman, S., Mukhopadhyay, D., Deloche, O., Wanke, V., Anrather, D., Ammerer, G., Riezman, H., et al. (2007). Sch9 is a major target of TORC1 in *Saccharomyces cerevisiae*. Mol. Cell *26*, 663–674.

Varlakhanova, N.V., Tornabene, B.A., and Ford, M.G.J. (2018). Feedback regulation of TORC1 by its downstream effectors Npr1 and Par32. Mol. Biol. Cell *29*, 2751–2765.

Wanke, V., Pedruzzi, I., Cameroni, E., Dubouloz, F., and De Virgilio, C. (2005). Regulation of G_0 entry by the Pho80-Pho85 cyclin-CDK complex. EMBO J. *24*, 4271–4278.

Wanke, V., Cameroni, E., Uotila, A., Piccolis, M., Urban, J., Loewith, R., and De Virgilio, C. (2008). Caffeine extends yeast lifespan by targeting TORC1. Mol. Microbiol. *69*, 277–285.

Wen, X., and Klionsky, D.J. (2016). An overview of macroautophagy in yeast. J. Mol. Biol. *428*, 1681–1699.

Wiśniewski, J.R., Zougman, A., Nagaraj, N., and Mann, M. (2009). Universal sample preparation method for proteome analysis. Nat. Methods *6*, 359–362.

Xue, L., Wang, P., Cao, P., Zhu, J.K., and Tao, W.A. (2014). Identification of extracellular signal-regulated kinase 1 (ERK1) direct substrates using stable isotope labeled kinase assay-linked phosphoproteomics. Mol. Cell. Proteomics *13*, 3199–3210.

Yamamoto, H., Fujioka, Y., Suzuki, S.W., Noshiro, D., Suzuki, H., Kondo-Kakuta, C., Kimura, Y., Hirano, H., Ando, T., Noda, N.N., and Ohsumi, Y. (2016). The Intrinsically Disordered Protein Atg13 Mediates Supramolecular Assembly of Autophagy Initiation Complexes. Dev. Cell *38*, 86–99.

Yang, H., Rudge, D.G., Koos, J.D., Vaidialingam, B., Yang, H.J., and Pavletich, N.P. (2013). mTOR kinase structure, mechanism and regulation. Nature *497*, 217–223.

Yeh, Y.Y., Wrasman, K., and Herman, P.K. (2010). Autophosphorylation within the Atg1 activation loop is required for both kinase activity and the induction of autophagy in *Saccharomyces cerevisiae*. Genetics *185*, 871–882.

Yerlikaya, S., Meusburger, M., Kumari, R., Huber, A., Anrather, D., Costanzo, M., Boone, C., Ammerer, G., Baranov, P.V., and Loewith, R. (2016). TORC1 and TORC2 work together to regulate ribosomal protein S6 phosphorylation in *Saccharomyces cerevisiae*. Mol. Biol. Cell *27*, 397–409.

Yi, C., Tong, J., Lu, P., Wang, Y., Zhang, J., Sun, C., Yuan, K., Xue, R., Zou, B., Li, N., et al. (2017). Formation of a Snf1-Mec1-Atg1 Module on Mitochondria Governs Energy Deprivation-Induced Autophagy by Regulating Mitochondrial Respiration. Dev. Cell *41*, 59–71.e54.

Zarei, M., Sprenger, A., Rackiewicz, M., and Dengjel, J. (2016). Fast and easy phosphopeptide fractionation by combinatorial ERLIC-SCX solid-phase extraction for in-depth phosphoproteome analysis. Nat. Protoc. *11*, 37–45.

Zhou, M., Meng, Z., Jobson, A.G., Pommier, Y., and Veenstra, T.D. (2007). Detection of in vitro kinase generated protein phosphorylation sites using γ [$^{18}O_4$]-ATP and mass spectrometry. Anal. Chem. *79*, 7603–7610.

Zhu, H., Klemic, J.F., Chang, S., Bertone, P., Casamayor, A., Klemic, K.G., Smith, D., Gerstein, M., Reed, M.A., and Snyder, M. (2000). Analysis of yeast protein kinases using protein chips. Nat. Genet. *26*, 283–289.

Zhu, H., Bilgin, M., Bangham, R., Hall, D., Casamayor, A., Bertone, P., Lan, N., Jansen, R., Bidlingmaier, S., Houfek, T., et al. (2001). Global analysis of protein activities using proteome chips. Science *293*, 2101–2105.

STAR★METHODS

KEY RESOURCES TABLE

REAGENT or RESOURCE	SOURCE	IDENTIFIER
Antibodies		
anti-Atg13-pSer^{554}	De Virgilio Lab	N/A
anti-HA	Sigma-Aldrich	11583816001; RRID:AB_514505
Bacterial and Virus Strains		
E. coli Rosetta (DE3)	Novagen	70954
E. coli DH5α	CGSC	12384
Chemicals, Peptides, and Recombinant Proteins		
Protease Complete Inhibitor Cocktail Tablets	Roche	11-697-498-001
GSH Beads	GE Healthcare	1707-5605
Ni-NTA Beads	QIAGEN	30210
Arg10	Sigma-Aldrich	608033
Arg6	Sigma-Aldrich	643440
Lys4	Sigma-Aldrich	616192
Lys8	Sigma-Aldrich	608041
PhosSTOP	Roche	04-906-837-001
Rapamycin	LC Laboratories	R-5000
TFA	Sigma-Aldrich	302031-100ML
Titanium dioxide	GL Sciences	5020-75010
Trypsin	Promega	V5113
Wortmannin	LC Laboratories	W-2990
γ-[$^{18}O_4$]-ATP	Cambridge Isotope Laboratories	OLM-7858-20
10 kD MW cutoff filter	PALL	OD010C34
C8 disc	3M Empore	14-386
C18 disc	3M Empore	14-386-2
Lys-C	FUJIFILM Wako Pure Chemical Corporation	129-02541
HR-X Column	Macherey-Nagel	730936P45
C18 Cartridges	Macherey-Nagel	731802
MS-grade Water	VWR	23595.328
MS-grade Acetonitrile	VWR	20060.320
C18 Column for High pH Fractionation	Waters	186003034
Pierce Anti-HA Magnetic Beads	Thermo Scientific	88837
Pefabloc	Sigma-Aldrich	76307
Lambda Protein Phosphatase	NEB	P0753L
Protein MettaloPhosphatases Buffer	NEB	B0761
α-Naphthyl Phosphate Disodium Salt	Sigma-Aldrich	N7255
Critical Commercial Assays		
Pierce BCA Protein Assay Kit	Thermo Scientific	23227
ECL Western Blotting Detection	GE Healthcare	RPN2106
Deposited Data		
MS-RAW files	ProteomeXchange	PXD013271
Experimental Models: Organisms/Strains		
TB50a	Schmelzle et al., 2004	MATa; *trp1, his3, ura3-52, leu2-3,112, rme1*
RL170-2C (Figures S2 and S3)	Hatakeyama et al., 2019	[TB50a] *TCO89-TAP::TRP1*
BY4741 (Figures S2 and S3)	Euroscarf	*MATa; his3Δ1, leu2Δ0, met15Δ0, ura3Δ0*

(*Continued on next page*)

Continued

REAGENT or RESOURCE	SOURCE	IDENTIFIER
Y14547 (Figures S2 and S3)	Euroscarf	[BY4741] *atg1Δ::kanMX4*
MP5102 (Figures S2 and S3)	Euroscarf	[BY4741] *atg13Δ::kanMX4*
Y258 (Figures S2 and S3)	Zhu et al., 2001	*MATa; his4-580, leu2-3,112, ura3-52, pep4-3*
SR5190 (Figures S2 and S3)	Open Biosystems	[Y258] pBG1805-*GAL1-ATG2-TAP*
SR5192 (Figures S2 and S3)	Open Biosystems	[Y258] pBG1805-*GAL1-ATG3-TAP*
SR5194 (Figures S2 and S3)	Open Biosystems	[Y258] pBG1805-*GAL1-ATG5-TAP*
SR5195 (Figures S2 and S3)	Open Biosystems	[Y258] pBG1805-*GAL1-ATG6-TAP*
SR5193(Figures S2 and S3)	Open Biosystems	[Y258] pEGH-*GAL1-GST-ATG4*
SR5196 (Figures S2 and S3)	Open Biosystems	[Y258] pEGH-*GAL1-GST-ATG7*
SR5197 (Figures S2 and S3)	Open Biosystems	[Y258] pEGH-*GAL1-GST-ATG8*
SR5198 (Figures S2 and S3)	Open Biosystems	[Y258] pEGH-*GAL1-GST-ATG9*
SR5199 (Figures S2 and S3)	Open Biosystems	[Y258] pEGH-*GAL1-GST-ATG10*
SR5200 (Figures S2 and S3)	Open Biosystems	[Y258] pBG1805-*GAL1-ATG11-TAP*
SR5201 (Figures S2 and S3)	Open Biosystems	[Y258] pEGH-*GAL1-GST-ATG12*
SR5202 (Figures S2 and S3)	Open Biosystems	[Y258] pEGH-*GAL1-GST-ATG13*
SR5203 (Figures S2 and S3)	Open Biosystems	[Y258] pEGH-*GAL1-GST-ATG14*
SR5204 (Figures S2 and S3)	Open Biosystems	[Y258] pBG1805-*GAL1-ATG15-TAP*
SR5205 (Figures S2 and S3)	Open Biosystems	[Y258] pEGH-*GAL1-GST-ATG16*
SR5206 (Figures S2 and S3)	Open Biosystems	[Y258] pEGH-*GAL1-GST-ATG17*
SR5207 (Figures S2 and S3)	Open Biosystems	[Y258] pBG1805-*GAL1-ATG18-TAP*
SR5208 (Figures S2 and S3)	Open Biosystems	[Y258] pBG1805-*GAL1-ATG19-TAP*
SR5209 (Figures S2 and S3)	Open Biosystems	[Y258] pBG1805-*GAL1-ATG20-TAP*
SR5210 (Figures S2 and S3)	Open Biosystems	[Y258] pBG1805-*GAL1-ATG21-TAP*
SR5211 (Figures S2 and S3)	Open Biosystems	[Y258] pBG1805-*GAL1-ATG22-TAP*
SR5212 (Figures S2 and S3)	Open Biosystems	[Y258] pEGH-*GAL1-GST-ATG23*
SR5213 (Figures S2 and S3)	Open Biosystems	[Y258] pEGH-*GAL1-GST-SNX4*
SR5214 (Figures S2 and S3)	Open Biosystems	[Y258] pBG1805-*GAL1-ATG26-TAP*
SR5215 (Figures S2 and S3)	Open Biosystems	[Y258] pBG1805-*GAL1-ATG27-TAP*
SR5216 (Figures 4F, S2, and S3)	Open Biosystems	[Y258] pEGH-*GAL1-GST-ATG29*
SR5217 (Figures S2 and S3)	Open Biosystems	[Y258] pBG1805-*GAL1-ATG31-TAP*
SR5218 (Figures S2 and S3)	Open Biosystems	[Y258] pEGH-*GAL1-GST-ATG32*
SR5219 (Figures S2 and S3)	Open Biosystems	[Y258] pBG1805-*GAL1-ATG33-TAP*
SR5220 (Figures S2 and S3)	Open Biosystems	[Y258] pBG1805-*GAL1-ATG34-TAP*
SR5221 (Figures S2 and S3)	Open Biosystems	[Y258] pBG1805-*GAL1-ATG36-TAP*
SR5222 (Figures S2 and S3)	Open Biosystems	[Y258] pBG1805-*GAL1-ATG38-TAP*
SR5223 (Figures S2 and S3)	Open Biosystems	[Y258] pBG1805-*GAL1-ATG39-TAP*
SR5224 (Figures S2 and S3)	Open Biosystems	[Y258] pEGH-*GAL1-GST-ATG40*
SR5225 (Figures S2 and S3)	Open Biosystems	[Y258] pEGH-*GAL1-GST-ATG41*
TS139 (Figures 4G and 4H)	Schmelzle et al., 2004	[TB50a] *pho8Δ60*
SR4934 (Figures 4G and 4H)	This study	[TB50a] *pho8Δ60, atg29Δ::kanMX*
SR4991 (Figures S2 and S3)	This study	[BY4741] *arg4Δ::URA3, lys2Δ, ATG29-3HA-kanMX*
MJ5682 (Figures S2 and S3)	This study	[BY4741] *arg4Δ::His3-MX6, lys2Δ::HphMX*
MJ5691 (Figures S2 and S3)	This study	[BY4741] *arg4Δ::His3-MX6, lys2Δ::HphMX, atg1Δ::kanMX*
Recombinant DNA		
p1613 (Figures S2 and S3)	Kawamata et al., 2008	[pRS316] *HA-ATG1*
p1614 (Figures S2 and S3)	Kawamata et al., 2008	[pRS316] *HA-atg1*^{D211A}
p3577 (Figure 4B)	Yamamoto et al., 2016	[pR316] *ATG13-2HA*

(*Continued on next page*)

Continued

REAGENT or RESOURCE	SOURCE	IDENTIFIER
p3632 (Figure 4B)	This study	[pRS416] *atg13*^{S554A}*-3HA*
p3425 (Figures 4G and 4H)	This study	[pRS416] *ATG29-3HA*
p3473 (Figures 4G and 4H)	This study	[pRS416] *atg29*^{3SA}*-3HA*
p3504 (Figures 4G and 4H)	This study	[pRS416] *atg29*^{T115A}*-3HA*
p3541 (Figures 4G and 4H)	This study	[pRS416] *atg29*^{T115E}*-3HA*
pRS413	Sikorski and Hieter, 1989	*CEN, ARS, HIS3*
pRS414	Sikorski and Hieter, 1989	*CEN, ARS, TRP1*
pRS415	Sikorski and Hieter, 1989	*CEN, ARS, LEU2*
pRS416	Sikorski and Hieter, 1989	*CEN, ARS, URA3*
Software and Algorithms		
ImageJ	NIH	https://imagej.nih.gov/ij/index.html
Photoshop	Adobe	https://www.adobe.com/
MaxQuant	Cox and Mann, 2008	https://maxquant.net/maxquant/
Perseus	Tyanova et al., 2016	https://maxquant.net/perseus/
Cytoscape	Shannon et al., 2003	https://cytoscape.org/
ClueGO	Bindea et al., 2009	http://apps.cytoscape.org/apps/cluego
Motif Analysis	NIH	https://www.phosphosite.org/staticMotifAnalysis.action
Sequence Logo	NIH	https://www.phosphosite.org/sequenceLogoAction.action

LEAD CONTACT AND MATERIALS AVAILABILITY

Further information and requests for resources and reagents, i.e., plasmids, yeast strains and antibodies generated in this study, should be directed to and will be fulfilled by the Lead Contact, Jörn Dengjel (joern.dengjel@unifr.ch). This study did not generate new unique reagents.

EXPERIMENTAL MODEL AND SUBJECT DETAILS

Yeast strains, plasmids, and growth conditions

Saccharomyces cerevisiae strains and plasmids are listed in Table S5. Unless otherwise stated, yeast strains were grown to mid log phase in SD medium (0.17% yeast nitrogen base, 0.5% ammonium sulfate and 2% glucose). SD medium lacking ammonium sulfate and amino acids was used to starve cells. For Atg protein purifications, we grew cells in medium containing 2% raffinose to OD_{600} of 0.5. Galactose was then added to a final concentration of 2% to induce the expression of proteins during 6 h, followed by rapamycin treatment (200 ng/mL) for 30 min. Cells were collected, lysed in buffer containing 100 mM TRIS pH7.5, 300 mM NaCl, 1% NP40 and 1x proteases inhibitors (Roche), and either purified with GSH or Ni-NTA beads (GE) as in Zhu et al. (2000).

Sample preparation of *in vivo* SILAC experiments

The yeast strains were grown in synthetic dextrose complete medium containing either non-labeled or labeled lysine and arginine variants: "Heavy" L-arginine-$^{13}C_6$-$^{15}N_4$ (Arg10) and L-lysine-$^{13}C_6$-$^{15}N_2$ (Lys8), or "medium-heavy" L-arginine-$^{13}C_6$ (Arg6) and L-lysine-$^{2}H_4$ (Lys4) amino acids (Sigma-Aldrich) were used as labels. In total, ten SILAC experiments were performed using the following label scheme:

Experiment/Label	Light	Medium-Heavy	Heavy
ATG1_KO_1	KO-Rapa	WT+Rapa	KO+Rapa
ATG1_KO_2	KO+Rapa	KO-Rapa	WT+Rapa
ATG1_KO_3	WT+Rapa	KO+Rapa	KO-Rapa
ATG1_KO_4	KO-Rapa	WT+Rapa	KO+Rapa
ATG1_KO_5	KO+Rapa	KO-Rapa	WT+Rapa
WT_1	KO+Rapa	WT+Rapa	WT-Rapa

(*Continued on next page*)

Continued

Experiment/Label	Light	Medium-Heavy	Heavy
WT_2	WT-Rapa		WT+Rapa
WT_3	WT+Rapa		WT-Rapa
WT_4	WT-Rapa		WT+Rapa
WT_5	WT+Rapa		WT-Rapa

Cells were treated or not with 200 ng/mL rapamycin for 30 min. Dried TCA-treated cell pellets (50 mg) of each labeling were mixed. Cells were broken by glass beads in urea buffer (8 M urea, 50 mM Tris HCl (pH 8)). Debris was pelleted and the supernatant containing cellular proteins was collected. These steps were repeated 5 times to extract proteins. Proteins were reduced by 1 mM DTT, alkylated by 5 mM iodoacetamide and digested by Lys-C (Lysyl Endopeptidase, WAKO) for 4 h. The concentration of urea was diluted to 1 M before overnight trypsin digestion (Promega).

On the second day, the samples were acidified using 50% TFA (final concentration 0.5%) and centrifuged at 4000 rpm for 10 min to remove precipitations. Peptides were purified by SPE using HR-X columns in combination with C18 cartridges (Macherey-Nagel): Buffer A, 0.1% formic acid in deionized water; Buffer B, 80% acetonitrile and 0.1% formic acid in deionized water. Elutes were frozen in liquid nitrogen and lyophilized for overnight.

On the third day, peptides were fractionated by HpH reversed phase chromatography (Batth et al., 2014). The dry peptide powder was suspended in 400 μl 5% ammonium hydroxide and fractionated using a Waters XBridge BEH130 C18 3.5 μm 4.6 × 250 mm column on a Ultimate 3000 HPLC (Thermo Scientific). Peptides were injected with 0.1 μl/s. The flowrate of the mobile phase was 1 ml/min. HpH buffer A contained 10 mM ammonium formate in deionized water and buffer B contained 10 mM ammonium formate and 90% acetonitrile deionized water. Both buffers were adjusted to pH 10 with ammonium hydroxide. Peptides were fractionated by increasing acetonitrile concentration from 1% to 40% Buffer B in 25 min. 96 fractions were collected in a 96 deep well plate. Fractions were mixed with an interval of 12 to yield 12 final fractions. The peptides were acidified, frozen in liquid nitrogen and lyophilized for overnight. On the fourth day, the dry peptides were suspended in 200 μl 80% acetonitrile with 1% TFA for further phosphopeptide enrichment (see below).

METHOD DETAILS

Filter-Aided *In Vitro* Kinase Assay

For Atg1 assays, HA-tagged WT and kinase dead Atg1 were purified by immunoprecipitation using anti-HA magnetic beads (Thermo Scientific). The beads were directly used for *in vitro* kinase assay. For TORC1 assays (Hatakeyama et al., 2019), to obtain maximal TORC1 activity, 30 μg of purified TORC1 was incubated with 1 mM $MnCl_2$ for 30 min. As a negative control, purified TORC1 was inhibited with 6 μM wortmannin for 30 min. Atg proteins purified from yeast (Gelperin et al., 2005; Zhu et al., 2000) and TORC1 or Atg1 variants were added onto 10 kD MW-cutoff filters (Pall) and incubated for 1 h at 30°C in kinase buffer: 50 mM HEPES (pH 7.4), 150 mM NaCl, 0.625 mM DTT, PhosSTOP, 6.25 mM $MgCl_2$, and 1.8 mM γ-[$^{18}O_4$]-ATP (Cambridge Isotope Laboratory). The assay was stopped by the addition of 8 M urea and 1 mM DTT. Protein digestion for MS analysis was performed overnight according to the FASP protocol (Wiśniewski et al., 2009). On day 2, peptides were eluted twice with 100 μL 50 mM ammonium bicarbonate into fresh tubes. Eluates were acidified with TFA to a final concentration of 1% prior phosphopeptide enrichment.

Phosphopeptide Enrichment

For both *in vitro* and *in vivo* experiments, phosphopeptides were enriched by TiO_2 beads (GL Sciences), which were incubated with 300 mg/mL lactic acid in 80% acetonitrile, 1% TFA prior experiments (Zarei et al., 2016). Samples were incubated with a 2 mg TiO_2 slurry for 30 min at room temperature. For peptide elution, TiO_2 beads were transferred to 200 μL pipette tips, which were blocked by C8 discs (3M Empore). Tips were sequentially washed with 10% acetonitrile/1% TFA, 80% acetonitrile/1% TFA, and LC-MS grade water. Phosphopeptides were eluted with 50 μL of 5% ammonia in 20% acetonitrile and 50 μL of 5% ammonia in 80% acetonitrile. Eluates of single fractions were mixed and acidified with 20 μL of 10% formic acid. Samples were concentrated by vacuum concentration and resuspended in 20 μL of 0.1% formic acid for LC-MS/MS analysis. The tip flow-through was stored at −80°C for non-phosphopeptide analysis.

LC-MS/MS Analyses

LC-MS/MS measurements were performed on a QExactive (QE) Plus and HF-X mass spectrometer coupled to an EasyLC 1000 and EasyLC 1200 nanoflow-HPLC, respectively (all Thermo Scientific). Peptides were fractionated on a fused silica HPLC-column tip (I.D. 75 μm, New Objective, self-packed with ReproSil-Pur 120 C18-AQ, 1.9 μm (Dr. Maisch) to a length of 20 cm) using a gradient of

A (0.1% formic acid in water) and B (0.1% formic acid in 80% acetonitrile in water): samples were loaded with 0% B with a flow rate of 600 nL/min; peptides were separated by 5%–30% B within 85 min with a flow rate of 250 nL/min. Spray voltage was set to 2.3 kV and the ion-transfer tube temperature to 250°C; no sheath and auxiliary gas were used. Mass spectrometers were operated in the data-dependent mode; after each MS scan (mass range m/z = 370 – 1750; resolution: 70'000 for QE Plus and 120'000 for HF-X) a maximum of ten, or twelve MS/MS scans were performed using a normalized collision energy of 25%, a target value of 1'000 (QE Plus)/5′000 (HF-X) and a resolution of 17'500 for QE Plus and 30'000 for HF-X. MS raw files were analyzed using MaxQuant (version 1.6.2.10) (Cox and Mann, 2008) using a Uniprot full-length *S. cerevisiae* database (March, 2016) and common contaminants such as keratins and enzymes used for in-gel digestion as reference. Carbamidomethylcysteine was set as fixed modification and protein amino-terminal acetylation, serine-, threonine- and tyrosine- (heavy) phosphorylation, and oxidation of methionine were set as variable modifications. The MS/MS tolerance was set to 20 ppm and three missed cleavages were allowed using trypsin/P as enzyme specificity. Peptide, site, and protein FDR based on a forward-reverse database were set to 0.01, minimum peptide length was set to 7, the minimum score for modified peptides was 40, and minimum number of peptides for identification of proteins was set to one, which must be unique. The "match-between-run" option was used with a time window of 0.7 min. MaxQuant results were analyzed using Perseus (Tyanova et al., 2016).

ALP assays for the determination of autophagic flux and immunoblot analysis

Autophagy was induced by shifting the cells for 3 h to nitrogen starvation medium according to Noda et al. (1995). Autophagic flux was determined according to Klionsky et al. (2016). For immunoblot analyses, cell lysates were prepared as previously described (Hatakeyama et al., 2019) and subjected to SDS-PAGE and immunoblotting experiments using the indicated antibodies. Anti-Atg13-pSer^{554} antibodies were generated by GenScript. Yeast cells expressing plasmid-encoded Atg13-2HA were collected and resuspended in lysis buffer (5 mM EDTA, 1% Triton X-100, protease inhibitor cocktail [Roche], Pefabloc [Sigma-AldrFich] and PhosSTOP [Roche] in phosphate-buffered saline), and disrupted with glass beads using a Precellys homogenizer. Atg13-2HA was purified by incubation with anti-HA magnetic beads (Pierce) and washed with lysis buffer. The beads were further washed with, and then resuspended in Protein MettalloPhosphatases buffer (NEB) supplemented with 1 mM $MnCl_2$ and incubated in the presence or absence of Lambda protein phosphatase (NEB) for 30 min at 30°C. The samples were incubated in Laemmli sample buffer for 10 min at 65°C and subjected to SDS-PAGE and immunoblot analysis.

QUANTIFICATION AND STATISTICAL ANALYSIS

We combined the measurement of the log2 fold change on each site and for the 15 replicates into a random effect model. Specifically, we considered *a priori* the sites as a random effect and we included the variability among replicates by also considering the replicates as a random effect. The model reads as

$$y_{ij} = a + s_i + r_j + \varepsilon_{ij}$$

where y_{ij} is the log2 fold change at the site *i* and for the replicate *j*. The variable s_i represents the log2fold change a site *i*, for which the potential variability among the replicates, the term r_j, has been taken into account. The model assumes a common intercept *a* and residuals ε_{ij}. The model has been fitted to the data using the function *lmer* of the library *lme4* (Bates et al., 2015) in the statistical software R (R Team, 2019).

Then, a posterior, we extracted the *average* effect size in log2 fold change and its *standard error* effect size for each site. This is done by the function *ranef* of the library *lme4*. From these posterior values, each site is assigned an average effect size and its corresponding 95% confidence interval:

$$\textit{average effect size} \pm qt(0.975, d.f. = \textit{number of replicates at a given site})\ \text{X}\ \textit{standard error}.$$

The value *qt* represents the *0.975* quantile of the Student distribution for a degree of freedom of *d.f.*, so that the exact number of replicates available for a given site is taken into account into the computation of the confidence interval. If the confidence interval includes values of zeros, then there is no statistically significant log2 fold change, whereas if the confidence interval is above (below) zeros, then there is statistical evidence for upregulation (downregulation) (see Figure 2A).

GO-term analyses were performed with Cytoscape 3.7.1 (Shannon et al., 2003) and ClueGO 2.5.3. (Bindea et al., 2009). Ontology enrichment (background: genome) was calculated using those genes, whose proteins carried phosphosites that were min. 2-fold regulated, either positive or negative. GO-biological process (BP), -cellular component (CC) and KEGG were selected for calculations. GO term fusion was used. Only pathways with a p value $\leq$ 0.05 were determined as significant (Bonferroni corrected). GO tree interval was set between 4 and 8. GO clusters contained at least 5 genes or 10% of all input genes. Enrichment/depletion (two-sided hypergenometric test) and Bonferroni p value correction were selected for statistical analyses. Sequence logos and motif analyses were performed using the service of the PhosphoSitePlus® website. The background for both calculations was based on the respective input sequences. Motifs with a p value $\leq$ 0.001 and a support threshold $\geq$ 0.05 were selected. To identify the maximum number of identifiable phosphosites we fitted the cumulative sum of

newly identified phosphosites per experiment with a least square optimization using Excel. Homolog sequences alignments were performed with Clustal Omega, a web tool of EMBL-EBI, using default settings (Madeira et al., 2019). Proteins homologs were extracted from UniProt.

DATA AND CODE AVAILABILITY

The mass spectrometry proteomics data have been deposited to the ProteomeXchange Consortium via the PRIDE partner repository with the dataset identifier PRIDE Archive: PXD013271 (Perez-Riverol et al., 2019).